

Cerebral haemodynamics in patients with glutaryl-coenzyme A dehydrogenase deficiency

Kevin A. Strauss,^{1,2,3} Patrick Donnelly¹ and Max Wintermark⁴

1 Clinic for Special Children, Strasburg, PA, USA

2 Department of Biology, Franklin and Marshall College, Lancaster, PA, USA

3 Lancaster General Hospital, Lancaster, PA, USA

4 Neuroradiology Section, University of California, San Francisco, CA, USA

Correspondence: Kevin A. Strauss, MD,

Clinic for Special Children,

535 Bunker Hill Road,

Strasburg, PA 17579,

USA

E-mail: kstrauss@clinicforspecialchildren.org

In glutaric aciduria type 1, glutaryl-coenzyme A and its derivatives are produced from intracerebral lysine and entrapped at high concentrations within the brain, where they interfere with energy metabolism. Biochemical toxicity is thought to trigger stroke-like striatal degeneration in susceptible children under 2 years of age. Here, we explore vascular derangements that might also contribute to brain damage. We studied injured and non-injured Amish glutaric aciduria type 1 patients using magnetic resonance imaging ($n=26$), transcranial Doppler ultrasound ($n=35$) and perfusion computed tomography ($n=6$). All glutaric aciduria type 1 patients had wide middle cerebral, internal carotid and basilar arteries. In non-injured patients, middle cerebral artery velocities were 18–26% below control values throughout late infancy and early childhood, whereas brain-injured children had an early velocity peak (18 months) and low values thereafter. Perfusion scans from six patients showed that tissue blood flow did not undergo a normal developmental surge. We observed four different perfusion patterns. (i) Three children (two non-injured) had low cerebral blood flow, prolonged mean transit time, elevated cerebral blood volume and high mean transit time/cerebral blood flow and cerebral blood volume/cerebral blood flow ratios. This pattern optimizes substrate extraction at any given flow rate but indicates low perfusion pressure and limited autoregulatory reserve. (ii) Ten hours after the onset of striatal necrosis in an 8-month-old infant, mean transit time and cerebral blood volume were low relative to cerebral blood flow, which varied markedly from region to region. This pattern indicates disturbed autoregulation, regional perfusion pressure gradients, or redistribution of flow from functional capillaries to non-exchanging vessels. (iii) In an infant with atrophic putaminal lesions, striatal flow was normal but mean transit time and cerebral blood volume were low, consistent with perfusion in excess of metabolic demand. (iv) Finally, a brain-injured adult with glutaric aciduria type 1 had regional perfusion values within the normal range, but the putamina, which normally have the highest regional perfusion, had cerebral blood flow values 24% below cortical grey matter. Although metabolic toxicity appears central to the pathophysiology of striatal necrosis, cerebrovascular changes probably also contribute to the process. These changes may be the primary cause of expanded cerebrospinal fluid volume in newborns, intracranial and retinal haemorrhages in infants and interstitial white matter oedema in children and adults. This pilot study suggests important new areas for clinical investigation.

Keywords: cerebral haemodynamics; glutaric aciduria type 1; perfusion computed tomography; striatal necrosis; transcranial Doppler ultrasound

Abbreviations: CBF=cerebral blood flow; CBV=cerebral blood volume; GA1=glutaric aciduria type 1; GCDH=glutaryl-CoA dehydrogenase; MCA=middle cerebral artery

Received July 1, 2009. Revised September 30, 2009. Accepted October 1, 2009

© The Author (2009). Published by Oxford University Press on behalf of the Guarantors of Brain. All rights reserved.

For Permissions, please email: journals.permissions@oxfordjournals.org

Introduction

Glutaryl-CoA dehydrogenase deficiency (glutaric aciduria type 1, GA1) is an autosomal recessive disorder of mitochondrial lysine and tryptophan degradation. It is prevalent among Old Order Amish of Lancaster County (Morton *et al.*, 1991) due to a 1262C>T (A421V) mutation in the gene coding for glutaryl-CoA dehydrogenase (*GCDH*). Glutaryl-CoA is proximal to the enzyme block and its derivatives (glutarate, 3-hydroxyglutarate and glutaryl-carnitine) accumulate in tissues, particularly the brain (Goodman *et al.*, 1977; Bennett *et al.*, 1986; Kolker *et al.*, 2003; Funk *et al.*, 2005).

Despite early diagnosis, one-third of affected Amish infants develop striatal lesions within medial and lateral lenticulostriate distributions of the middle cerebral artery (MCA) (Feekes and Cassell, 2006; Strauss *et al.*, 2007). Brain injury is often sudden, like a stroke. Even in cases of insidious motor delay, lesions may occur suddenly during antenatal or neonatal life only to become evident between 2 and 6 months of age (Strauss *et al.*, 2007).

The term 'metabolic stroke' has been applied to GA1 and other disorders in which a primary derangement of the tricarboxylic acid cycle or respiratory chain, rather than ischaemia, is thought to trigger neuronal necrosis (Hoffmann *et al.*, 1994; Haas *et al.*, 1995; Oppenheim *et al.*, 2000; Abe *et al.*, 2004; Strauss *et al.*, 2007). There is experimental evidence that some form of energy failure is central to the pathophysiology of GA1 (Kolker *et al.*, 2004; Sauer *et al.*, 2005; Strauss *et al.*, 2007; Zinnanti *et al.*, 2007). However, the only direct evidence of an energy disturbance in humans comes from fluorodeoxyglucose positron emission tomography studies of asymptomatic Amish infants showing glucose tracer uptakes reduced by 28, 27, 18 and 14% in putamen, caudate, thalamus and cortical grey matter, respectively (Strauss *et al.*, 2007).

Although these studies support the metabolic hypothesis of GA1, the physiology may be more complex. We have long recognized that expansion of cerebrospinal fluid (CSF) volume and intradural haemorrhages in affected infants might result from haemodynamic rather than metabolic mechanisms (Mandel *et al.*, 1991; Martinez-Lage, 1996; Strauss and Morton, 2003; Muhlhausen *et al.*, 2004; Hernandez-Palazon *et al.*, 2006; Strauss *et al.*, 2007), and a limited number of perfusion computed tomography (CT) scans suggest that cerebral blood volume (CBV) and mean transit time are elevated in some children. Based on these and other observations, we hypothesized that metabolic inhibition of brain tissue entrains haemodynamic changes (Strauss *et al.*, 2007).

Here, we explore how such changes might relate to brain metabolism, intracranial fluid dynamics, haemorrhage risk and striatal damage. Our study of the MCA was guided by a simple idea: if flow-metabolism coupling remains intact, a 14%–28% decrease of cerebral metabolism should be matched by similar decreases of blood velocity (Wahl and Schilling, 1993; Hudetz, 1997a). Based on Doppler results, we reanalysed perfusion scans (Strauss *et al.*, 2007) to understand the correlation between MCA flow and capillary perfusion. Our results suggest that cerebral toxicity caused by *GCDH* deficiency may induce a state of arteriolar dilation and increased CBV. This implicates cerebral venous

hypertension as a mechanism of CSF expansion, intradural haemorrhage and interstitial oedema, suggesting that perfusion pressure, like glucose delivery, might be an important treatment variable.

Patients and methods

Estimation of cerebral vessel cross-sectional area

The ethics review board of Lancaster General Hospital approved the study and parents consented to participation. We studied MRI scans of 26 patients with GA1 and 26 age-matched control subjects between birth and 30 months of age. Images were obtained with a Siemens 1.5T Symphony scanner (Siemens Medical Systems). DicomWorks imaging software (<http://dicom.online.fr/>) was used to measure the diameter of the middle cerebral, internal carotid and basilar arteries. To minimize error, vessels were measured end-on (sagittal view of the middle cerebral arteries, coronal view of the internal carotids within the cavernous sinus and axial view of the basilar artery; see Fig. 2, upper panels). Vessel cross-sectional area was calculated: cross-sectional area (in mm²) = $\pi(0.5d)^2$, where π equals 3.14 and d is vessel diameter in millimetres (i.e. $0.5d$ equals vessel radius).

The cross-sectional area of each MCA was determined relative to the combined cross-sectional areas of the major cerebral feeding vessels:

$$MCA_f = \frac{MCA}{(ICA_l + ICA_r + BA)}$$

where MCA_f is fractional MCA cross-sectional area relative to the sum of cross-sectional areas for the left internal carotid (ICA_l), right internal carotid (ICA_r) and basilar (BA) arteries. Values for relative cross-sectional area were log transformed to produce a normal distribution for statistical analyses.

Measurement of middle cerebral artery velocity

We performed transcranial colour Doppler ultrasound of the proximal MCA segment in 35 GA1 children ages 1 week to 14 years. Twenty-six children were Amish and homozygous for the *GCDH* 1262C>T mutation. Those remaining were compound heterozygous for various mutations in *GCDH*. Several children with GA1 were imaged at serial time points (e.g. Fig. 9, lower row), yielding a total of 95 transcranial colour Doppler studies.

Children with GA1 were grouped according to neurological disability: children who had dystonia and MRI-documented striatal lesions were designated 'injured' ($n=18$) and those who had normal motor development and function were designated 'non-injured' ($n=17$). All but one of the injured children had atrophic striatal lesions before being imaged (Strauss *et al.*, 2007). For one child (Case 2 below), acute striatal necrosis occurred during the course of the study and transcranial colour Doppler measurements were available before and after the event (Fig. 8, column C).

Control transcranial colour Doppler data were collected from 86 healthy age-matched Mennonite and Amish children, two-thirds of whom were siblings of GA1 patients. To account for normal developmental changes in cerebral blood velocity, we assigned transcranial colour Doppler measurements to six different age groups (0–3 months, 4–6 months, 7–12 months, 13–24 months, 2–6 years

and 7–14 years) (Supplementary Table 1) (Wintermark *et al.*, 2004). In Figs 4, 5, 7 and 9, age is depicted on a log₂ scale for graphical clarity.

All Doppler images were obtained by a single technician using an High Density Imaging 5000 ultrasound system (Philips Medical Company) equipped with a low frequency phased array transducer (P4-2) operated at 2 MHz in pulse wave mode. We assumed an insonation angle (θ) of 0°. Angle correction was not used; the true θ was estimated to be between 0 and 25°, yielding a maximum error of 9% (i.e. $1 - \cos 25^\circ$).

With the child supine, the transducer was oriented in the transverse plane over the thinnest portion of the temporal bone, cephalad to the zygomatic arch, to identify the circle of Willis and locate the proximal segment of the MCA. We measured peak systolic velocity (V_{sys}), end-diastolic velocity (V_{dia}), and time-averaged mean flow velocity (V_{mean}) in cm/s. These values were used to calculate pulsatility index (PI):

$$PI = \frac{(V_{\text{sys}} - V_{\text{dia}})}{V_{\text{mean}}}$$

Perfusion computed tomography

Perfusion data were obtained using a published protocol and analysed with PCT software (Wintermark *et al.*, 2001, 2004). CBV (ml/100 g) was divided by mean blood transit time (seconds) to calculate cerebral blood flow (CBF; in ml/100 g per minute) for nine grey matter regions (caudate, putamen, thalamus, frontal cortex, central and calcarine sulci and frontal, parietal, temporal and occipital cortices) and four subcortical white matter regions (frontal, parietal, occipital, temporal). The inverse mean transit time (in s⁻¹) was also used to construct Fig. 6 because it is intuitively similar to velocity and has a linear relation to CBF ($r_s = 0.82$, $P < 0.0001$).

Perfusion CT scanning was done on six GA1 patients: two non-injured (aged 12 and 20 months), three with atrophic striatal lesions (ages 5.5 months, 20 months and 25 years) and one 8-month-old child in acute cerebral crisis, 10 and 100 h after the onset of opisthotonus (Case 2) (Strauss *et al.*, 2007). Values from GA1 patients were compared with previously published control data from 53 children, ages 7 days to 18 years (28 male and 25 female) (Wintermark *et al.*, 2004). To account for perfusion changes during development, the control group was divided into four paediatric subsets matched closely for age to individual GA1 patients (Supplementary Table 2).

Data analyses

Statistical analyses were performed using Prism4 software (<http://www.graphpad.com>). Vessel cross-sectional area as a function of age was studied with least-squares linear regression according to the equation $y = Mx + b$, where y is calculated vessel cross-sectional area in mm², M is the regression coefficient (slope), x is age in months and b is the estimated cross-sectional area at birth (i.e. when $x = 0$). The value r^2 signifies the strength of association between age and vessel cross-sectional area. Left and right velocity and cross-sectional area measurements obtained from each patient were counted independently; i.e. the number of measurements was twice the number of subjects (Table 1). MCA velocity measurements were normally distributed within each of the six age designations listed in Supplementary Table 1. Within each age bracket, one-way analysis of variance (ANOVA) was used to compare Doppler data from three groups: control, GA1 non-injured and GA1 injured. For ANOVA P values < 0.05 , the Tukey post-test was used for pairwise comparisons. The association between CBF and mean transit time or CBV was studied with Spearman rank correlation and results are reported as Spearman correlation coefficients (r_s). The unpaired t -test with Welch's correction was used to study perfusion parameters between GA1 and age-matched control subjects. For case summaries 1 and 2, data represented as z scores were calculated as:

$$z = \frac{(\text{patient value} - \text{control mean})}{\text{control SD}}$$

Normal z scores are between -2 and $+2$.

Results

Two cases are summarized below to illustrate the characteristic disturbance of CSF volume and brain water in infants with GA1 (Case 1), as well as perfusion abnormalities recorded during an acute striatal injury (Case 2). These and other cases prompted the haemodynamic studies that follow:

Case 1: Increased cerebrospinal fluid volume and interstitial brain oedema

An infant with GA1 was born with a large head (head circumference 40 cm; $z = +4.6$), widely split cranial sutures, prominent

Table 1 Summary statistics for grey matter perfusion in control and GA1 subjects; mean (\pm SD) for n grey matter regions of interest

Age	Neurological status	GA1			n	Control			n^d
		MTT (s)	CBV (ml/100g)	CBF (ml/100g-min)		MTT (s)	CBV (ml/100g)	CBF (ml/100g-min)	
20 months	Non-injured	6.13 (0.52) ^a	6.46 (1.13)	66.7 (15.4) ^a	7	2.45 (0.69)	5.42 (1.86)	147.6 (83.0)	54
20 months	Chronic injury	6.53 (4.04) ^a	7.13 (1.51) ^c	77.2 (28.0) ^a	7	2.45 (0.69)	5.42 (1.86)	147.6 (83.0)	54
12 months	Non-injured	3.74 (0.32)	5.92 (0.54) ^c	95.5 (9.1) ^c	8	3.36 (2.31)	5.22 (1.82)	122.1 (82.6)	54
8 months	Acute injury, 10 h	2.94 (0.61) ^b	3.45 (0.58) ^a	75.5 (28.3)	8	4.35 (2.59)	5.92 (2.18)	100.0 (48.5)	45
8 months	Acute injury, 100 h	4.23 (0.81)	3.12 (0.69) ^a	45.4 (13.4) ^a	8	4.35 (2.59)	5.92 (2.18)	100.0 (48.5)	45
5.5 months	Chronic injury	3.57 (0.52) ^a	4.45 (0.73) ^a	74.9 (7.0)	8	7.95 (4.39)	6.90 (2.35)	70.1 (46.7)	72
25 years	Chronic injury	4.27 (0.60)	4.73 (0.25)	54.3 (7.7)	8	4.51 (1.41)	4.96 (1.70)	65.3 (37.5)	24

a Different than control, Welch's unpaired t -test $P < 0.0001$.

b $P < 0.001$.

c $P < 0.05$.

d Control n values represent measurements from nine grey matter regions for each individual. Thus $n = 54$ represents six control subjects.

scalp veins, a wide, bulging anterior fontanelle and normal neurological exam. A cranial MRI at 7 days of age showed increased extra-axial fluid, enlarged fourth ventricle and basal cisterns, middle cranial fossae fluid collections and blunted temporal lobes (Fig. 1). Apparent water diffusion was elevated

throughout the brain, especially in frontal and occipital centrum semiovale (2.17×10^{-3} to $2.29 \times 10^{-3} \text{ mm}^2/\text{s}$; normal for neonate $1.70 \pm 0.22 \times 10^{-3} \text{ mm}^2/\text{s}$) (Fig. 1D). A computed tomography venogram showed normal internal cerebral veins, normal sinuses and widely patent jugular foramina.

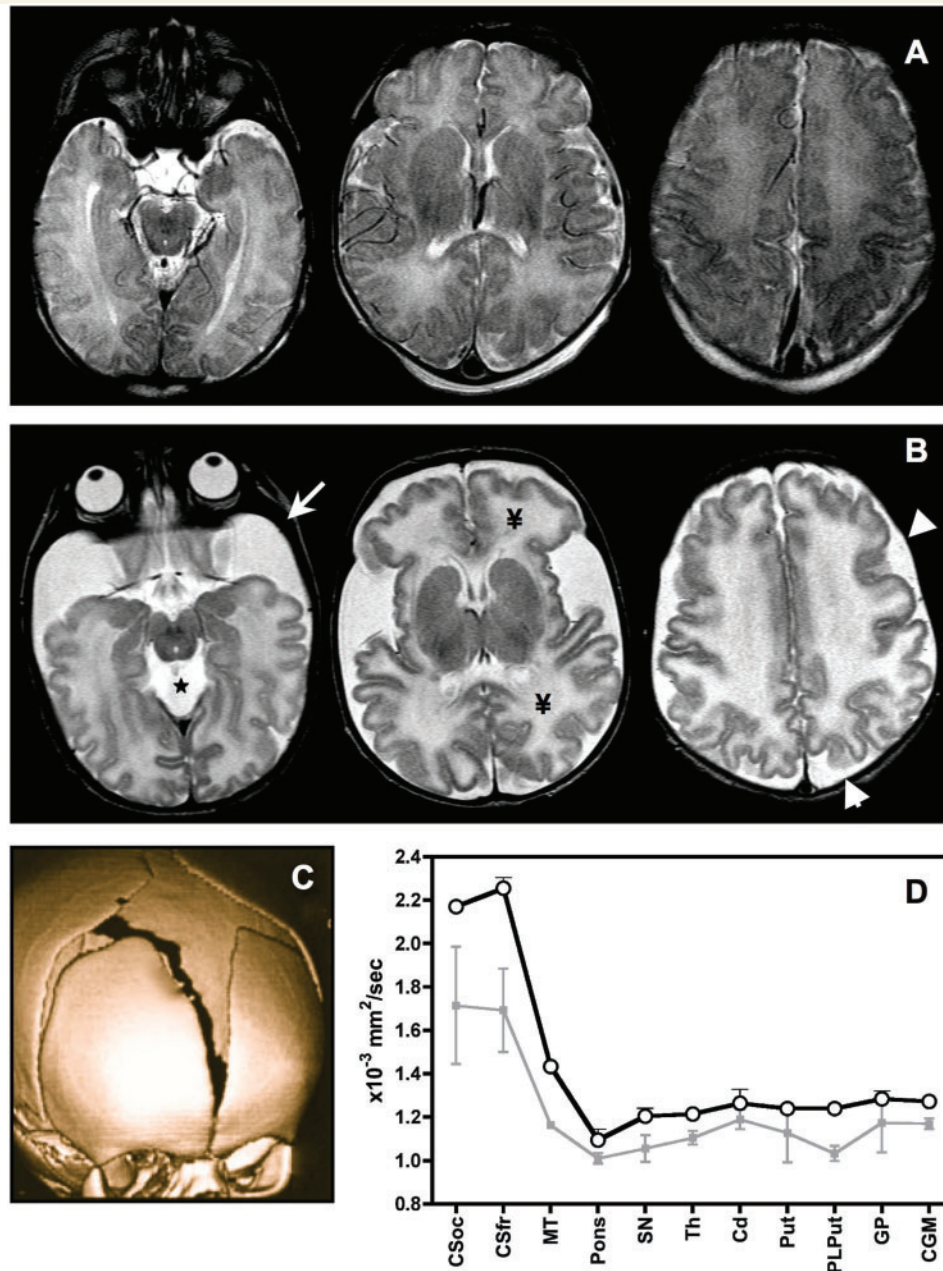


Figure 1 The brain MRI from a normal neonate (A) is compared with that from a 7-day-old neonate with GA1 (B). There are characteristic cysts within the middle cranial fossae (white arrow) and expanded CSF volume in the fourth ventricle (star), basal cisterns and over the cortical surface (white arrowheads). T₂ signal intensity and increased water diffusion are present in white matter regions of the centrum semiovale (¥). (C) The anterior fontanelle is large (CT reconstruction) and bulging. Opening pressure of the thecal sac was 28 cm H₂O (normal 19 ± 4 cm H₂O). (D) Water diffusion is slightly elevated in all brain regions. Grey squares represent normal mean (and SD) for healthy neonates. CSfr = centrum semiovale-frontal; CSoc = centrum semiovale-occipital; MT = large myelin tracks (average of middle cerebellar peduncle = genu and splenium of corpus callosum); Pons = dorsal pontine reticular formation; SN = substantia nigra; Th = thalamus; Cd = caudate; Put = anterior putamen; PLPut = posterior-lateral putamen; GP = globus pallidus; CGM = average of cortical, parietal, and occipital grey matter.

Cerebrospinal fluid opening pressure was 28 cm H₂O (normal 19.0 ± 4.4 cm H₂O; $z = +2$) with an amplitude of 16–30 cm H₂O (normal <5 cm H₂O).

Case 2: Acute striatal degeneration, low regional cerebral blood volume and signs of ischaemia

In a previous publication (Strauss *et al.*, 2007), we detailed the evolution of striatal injury in an Amish boy with GA1; his story is briefly summarized here. He was diagnosed with GA1 on his first day of life and treated with L-carnitine (80 mg/kg/day) and a lysine-restricted diet (lysine 71 ± 9 mg/kg/day, tryptophan 24 ± 4 mg/kg/day and lysine-free L-amino acids 0.5 g/kg/day). Head growth was stable along the 95th percentile. At age 6 months he had mild axial hypotonia and chorea of the distal upper limbs. At age 7 months he could not sit independently but could control his head and use his hands. At age 8 months, he developed sudden opisthotonus. A perfusion scan 10 h later showed low mean grey matter blood flow ($z = -0.5$), blood

volume ($z = -1.1$) and transit time ($z = -0.5$), with markedly variable perfusion from region to region (Fig. 2; see Table 1 for age-matched control values used to calculate z scores). For example, flow to the right putamen was only half that of adjacent caudate, but both values were still within a broad age-matched normal range ($z = -0.7$ and $+0.3$, respectively). MRI and CT scans 90 h later showed cytotoxic oedema (apparent water diffusion $0.64 \times 10^{-3} \text{ mm}^2/\text{s}$; $z = -4.2$) and reduced perfusion ($z = -1.2$) of striatal nuclei. Opening pressure of the thecal sac was 14 cm H₂O (normal 19.0 ± 4.4 cm H₂O). CSF neuron-specific enolase, a marker for neuronal lysis, was elevated (21.8 ng/ml; normal 3.5 ± 1.4 ng/ml). There was no biochemical evidence of encephalitis or blood-brain barrier dysfunction and spinal fluid glucose, lactate, amino acids and neurotransmitter metabolites were normal. Organic acid concentrations of CSF (glutamate 6.6 µmol/l, 3-hydroxyglutamate 0.45 µmol/l) were similar to those of plasma (glutamate 10.1 µmol/l, 3-hydroxyglutamate 0.53 µmol/l). The child made no motor progress over ensuing months. He had crippling dystonia by 1 year of age, when a repeat brain MRI showed severe striatal atrophy.

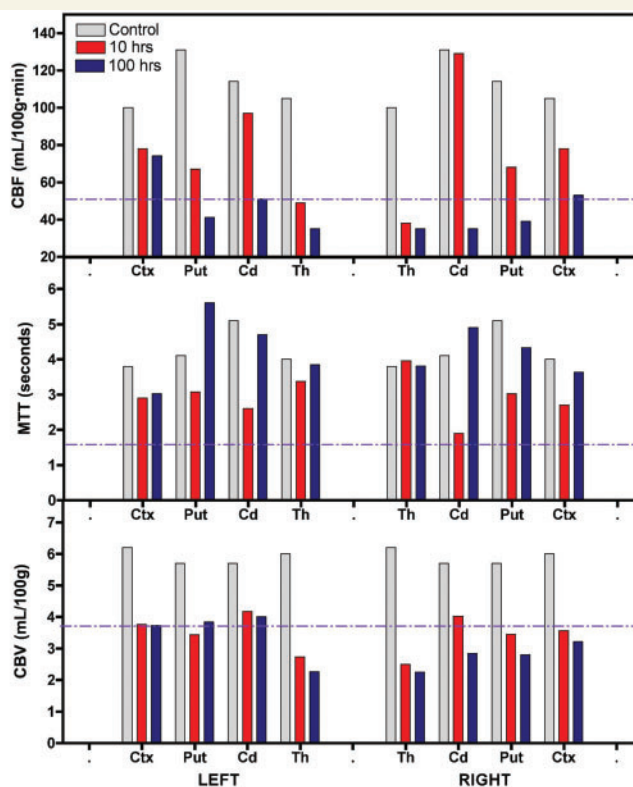
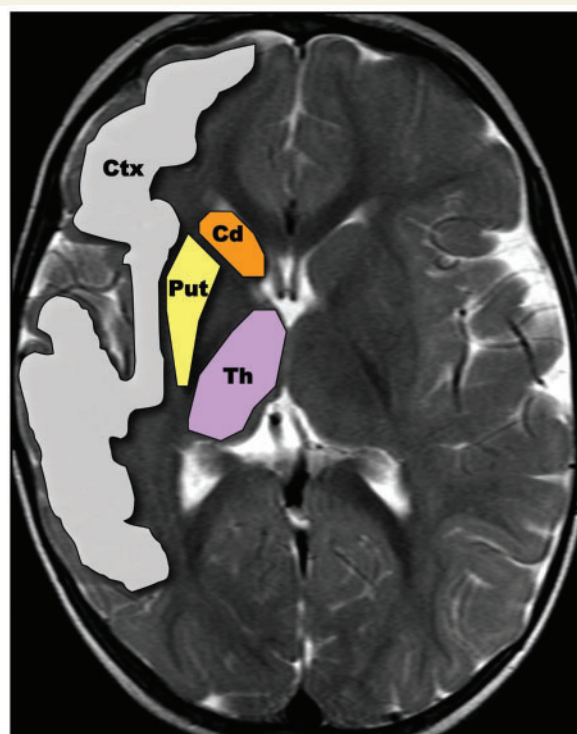


Figure 2 An 8-month-old Amish boy with GA1, compliant with diet and carnitine therapy, presented with acute opisthotonus. There was no precipitating illness. Perfusion parameters measured in multiple regions (left panel) at 10 h (red bars) and 100 h (blue bars) after the onset of dystonic posturing were compared with control regional mean values (grey bars; $n = 5$). Selected regions are ordered on the X-axis as they appear left to right across an axial section of the brain; dotted lines represent mean minus one standard deviation for nine grey matter regions measured in five control children age 8 ± 3 months ($n = 45$ total measurements). At 10 h, mean transit time (MTT) and CBV are relatively low and regional CBF is markedly heterogeneous. However, flows to the putaminae and caudates are within the normal range. At 100 h, CBVs are stable or diminished whereas mean transit times have increased, leading to frank ischaemia in deep grey matter structures, including putaminae. Cd = caudate nucleus; Ctx = frontal and parietal cortices; Put = putamen; Th = thalamus.

Vessel calibre

In children from all groups (control, GA1 injured and GA1 non-injured), cerebral feeding vessels, as depicted in Fig. 3, grew wider over the first 30 months of age (r^2 for MCA = 0.39 in control and 0.66 in GA1 subjects). Compared with control subjects, GA1 patients between 6 and 20 months of age had 34%–42% larger MCA ($P < 0.0001$) and 20%–49% larger combined vessel ($P < 0.0001$) cross-sectional area. Proportional cross-sectional area of the MCA [i.e. $MCA/(ICA_l + ICA_r + BA)$] was similar among groups, although there were outliers among injured patients (Fig. 3B).

Middle cerebral artery velocity

In control subjects, MCA velocity increased by 80% over the first few years of life and declined after age 6 (Fig. 4). In non-injured

GA1 patients, velocity did not surge but instead increased slowly to reach normal levels by age 6. The difference was greatest between 13 and 24 months of age, when mean velocity in GA1 children was 26% less than in controls ($P < 0.0001$). In brain-injured patients, MCA velocity peaked at ~18 months of age and was low thereafter. Velocity measurements overlapped among injured and non-injured GA1 children and varied considerably over time in each individual (Fig. 9, lower row). Thus, MCA velocity could not be reliably used to determine the risk for or presence of brain injury.

Pulsatility indices from both non-injured and injured GA1 children were similar to control values but differed significantly from each other during the second year of life (Fig. 5).

Regional grey matter perfusion

Perfusion data in Fig. 6 depict relationships of CBF to mean transit time, inverse mean transit time and CBV for nine grey matter and

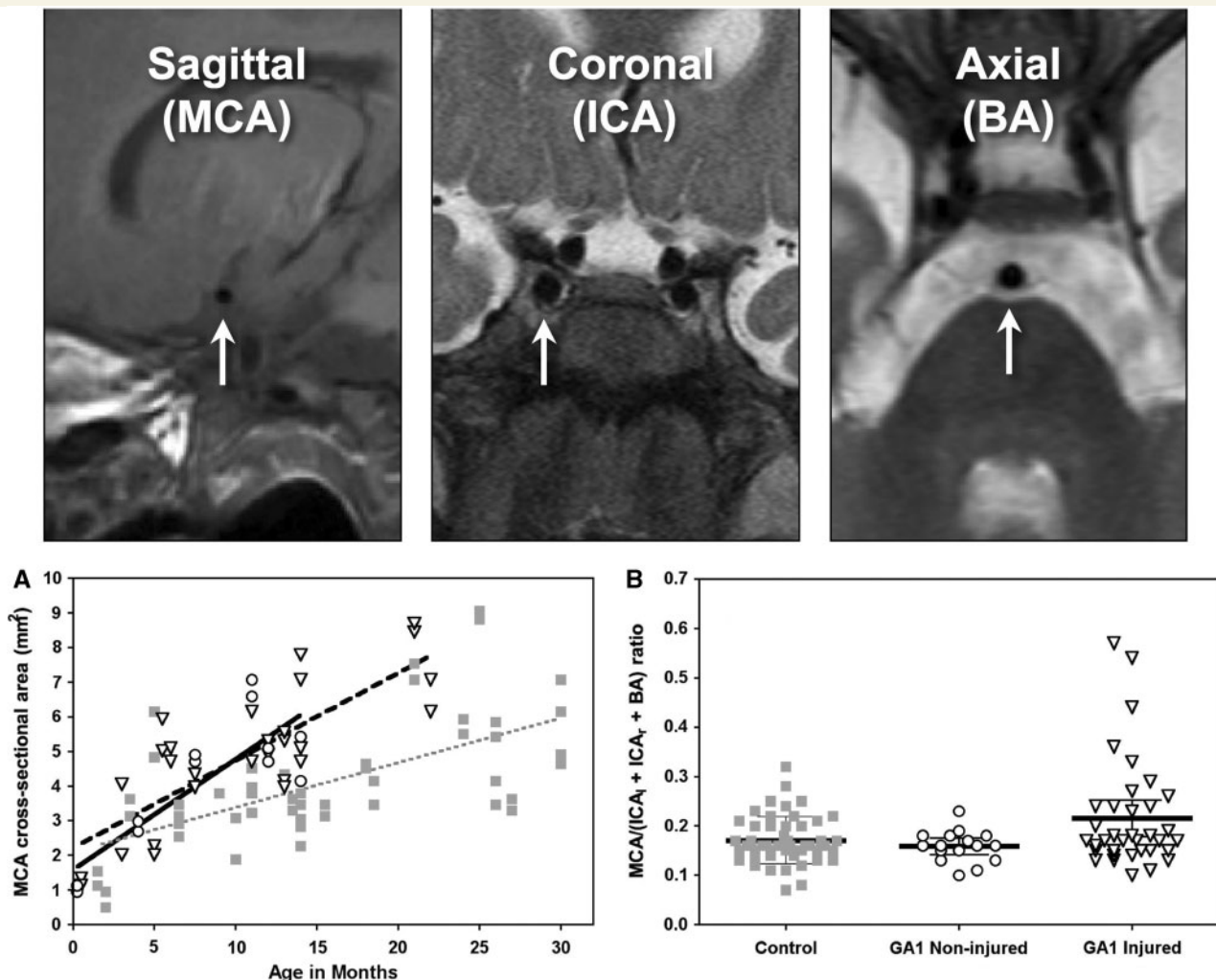


Figure 3 Upper panels show MRI slices used to measure cerebral vessels end-on (white arrows). From left to right: sagittal view of proximal MCA, coronal view of internal carotid arteries within the cavernous sinus and axial view of the basilar artery at the level of the pons and middle cerebellar peduncles. (A) MCA cross-sectional area (mm^2) as a function of age for control subjects (grey squares), healthy GA1 children (white circles) and brain-injured GA1 children (white triangles). MCA cross-sectional area was larger in children with GA1 regardless of injury status. A similar pattern was found for the internal carotid and basilar arteries (data not shown). (B) MCA cross-sectional area relative to the sum of internal carotid [left (ICl) and right (ICr)] and basilar (BA) cross-sectional areas did not differ among groups. However, this measurement was quite variable among brain-injured children.

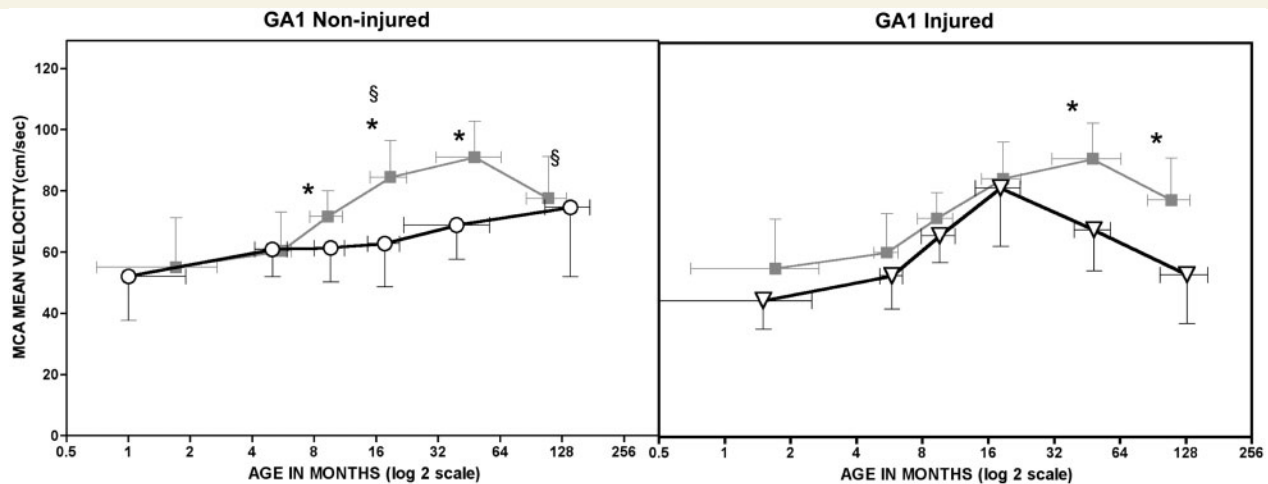


Figure 4 (A) Non-injured GA1 children (white circles) had a blunted velocity increase compared with controls (grey squares); mean velocity increased slowly to reach normal values later in childhood. (B) In brain-injured children (white triangles), velocity peaked between 16 and 18 months of age and then decreased below control values after age 2. Patterns for systolic and diastolic velocity were similar (data not shown). Age in months is plotted on a log₂ scale (*different than control; §different than GA1 injured).

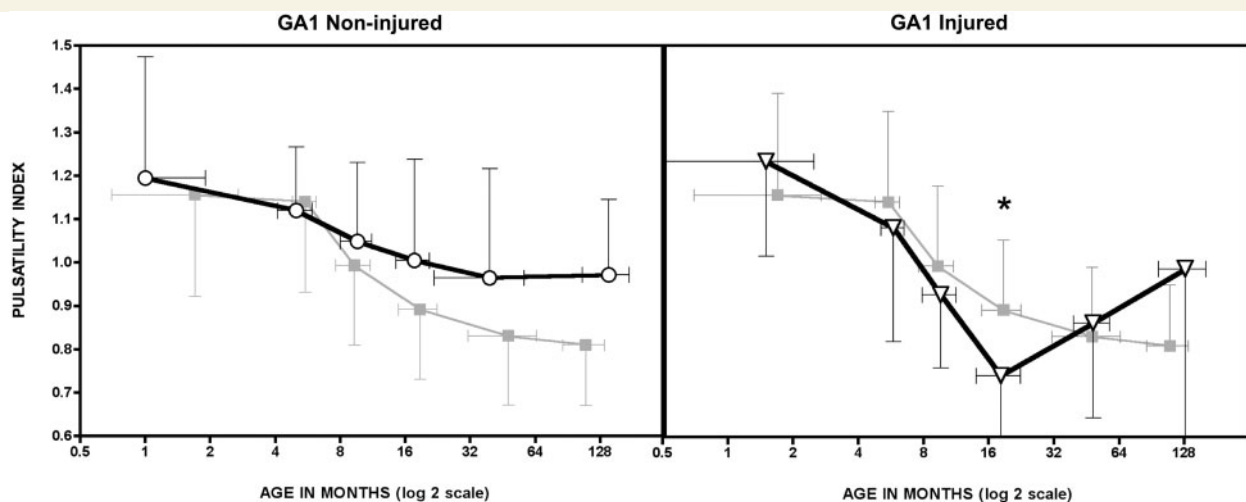


Figure 5 (A) In healthy children, pulsatility index $[PI = (V_{sys} - V_{dia})/V_{mean}]$ decreased over the first 10 years of life (grey squares; mean ± 1 SD), reflecting a progressive rise in perfusion pressure. MCA pulsatility for both non-injured (white circles) and injured (white triangles) GA1 patients was not statistically different from controls subjects. However, visual inspection reveals a less pronounced slope of the pulsatility index curve in non-injured patients. (B) In brain-injured children, pulsatility index decreased markedly during the second year of life, possibly indicating a transient change of perfusion pressure or cerebrovascular resistance. Age in months is plotted on a log₂ scale (*lower than GA1 healthy, ANOVA $P=0.001$, Tukey $P<0.01$).

four white matter regions among 53 control subjects ages 7 days to 18 years (Wintermark *et al.*, 2004). Blood flow correlated inversely with mean transit time ($r_s = -0.82$, $P<0.0001$) and had a linear relationship to inverse mean transit time ($r^2=0.65$, $P<0.0001$) suggesting that velocity is a strong determinant of flow. Blood flow correlated only weakly with CBV ($r_s=0.27$, $P<0.0001$) and there was no correlation between CBV and mean transit time.

Consistent with Doppler data, CBF did not surge in children with GA1 (Fig. 7). Among six patients, we observed four

different perfusion patterns (summarized in Table 1 and Figs 8–10):

- (i) High volume, slow velocity ($n=3$): A 12-month-old non-injured child had reduced CBF and elevated CBV. Mildly increased mean transit time was not statistically different from control (Table 1). Two 20-month-old girls, one injured and one non-injured, had low CBF, high CBV and high mean transit time in all grey matter regions; CBF varied considerably from region to region (Fig. 9A).

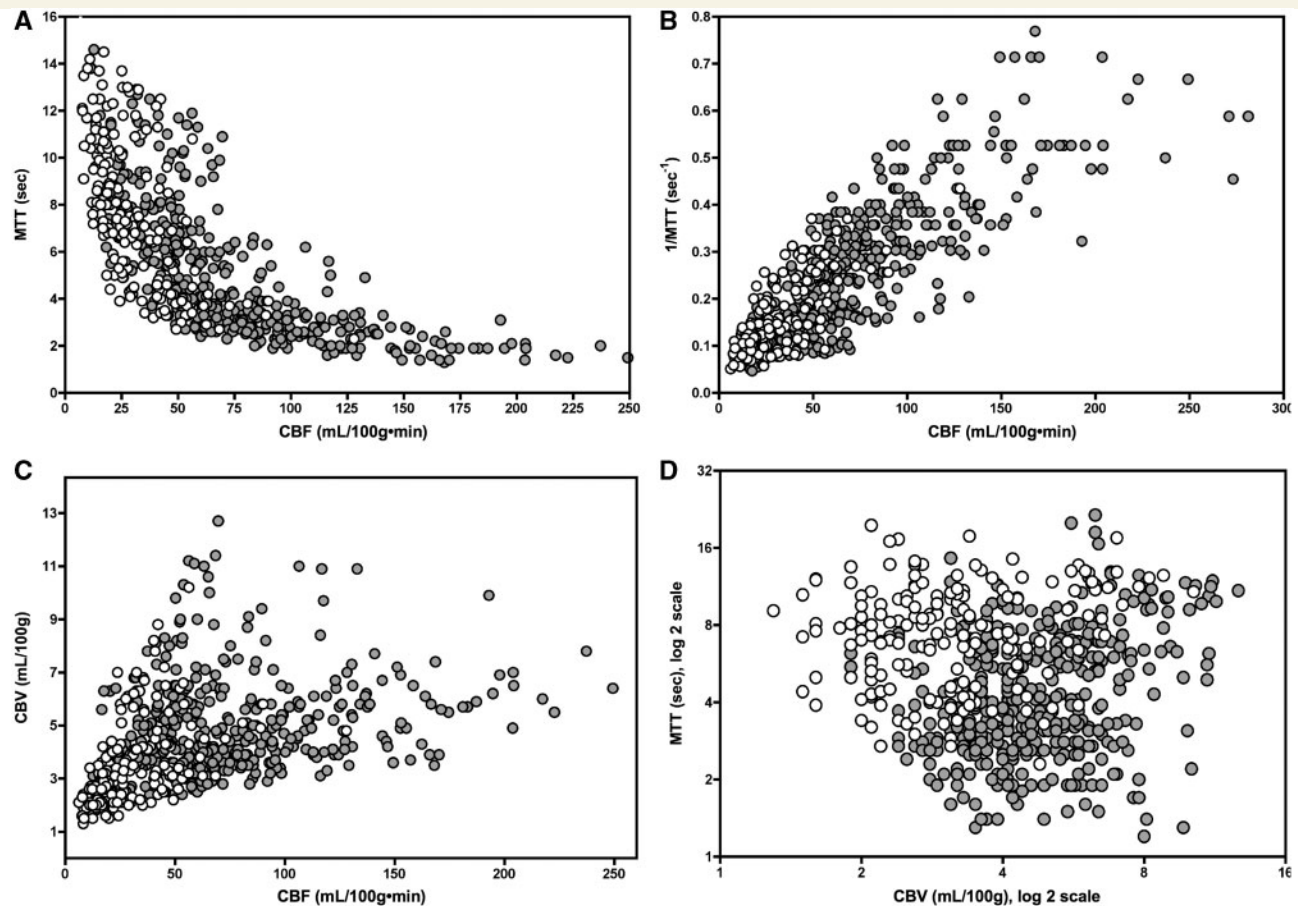


Figure 6 Perfusion CT measurements from nine grey matter regions (grey circles: caudate, putamen, thalamus, frontal cortex, central and calcarine sulci, and frontal, parietal, temporal and occipital cortices) and four subcortical white matter regions (white circles: frontal, parietal, occipital, temporal) among 53 control subjects ages 7 days to 18 years. CBF correlated inversely with mean transit time (MTT) ($r_s = -0.82$, $P < 0.0001$; **A**), was linearly related to inverse mean transit time ($1/MTT$) ($r^2 = 0.65$, $P < 0.0001$; **B**), and only weakly correlated to CBV ($r_s = 0.27$, $P < 0.0001$; **C**). There was no correlation between CBV and mean transit time (**D**).

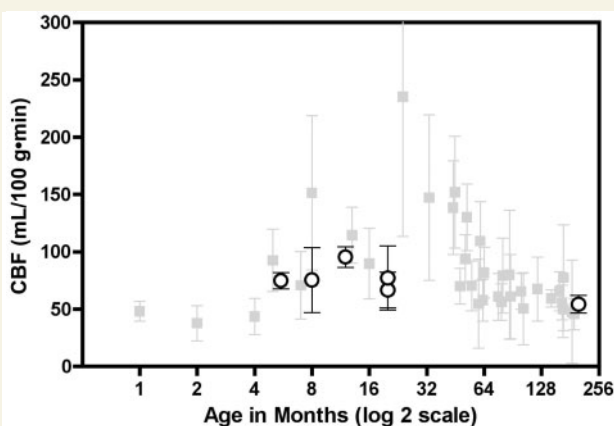


Figure 7 Grey squares show age-specific mean \pm SD perfusion CT blood flow measurements (in ml/100g·min) from nine grey matter regions among 53 control subjects aged 7 days to 18 years (data redrawn from Wintermark *et al.*, 2004). The developmental surge in perfusion was not observed in GA1 patients (white circles). Age in months is on a log₂ scale.

- (ii) Acute striatal injury—low volume, high velocity, heterogeneous perfusion ($n = 1$): An 8-month-old boy was imaged 10 and 100 h after the onset of an acute striatal injury (Case 2). At 10 h, mean transit time and CBV values were low (Table 1, Fig. 9B). Regional CBF values, although markedly heterogeneous, were within a broad age-appropriate range (Table 1). By 100 h into cerebral crisis, mean transit time normalized, CBV remained low and the striata and thalami were ischaemic (Fig. 2). Only the striata, however, subsequently degenerated.
- (iii) Chronic atrophic lesions—low volume, high velocity, homogeneous perfusion ($n = 1$): Regional CBFs were normal but both mean transit time and CBV values were low in a 5.5-month-old girl with chronic atrophic striatal lesions (Fig. 9C).
- (iv) Low putaminal blood flow ($n = 1$): A 25-year-old injured patient had tightly clustered CBF, CBV and mean transit time values within the adult normal range (Table 1). However, CBF in gliotic putamen was 24% below values in cortex.

These patterns are more clearly differentiated in Fig. 10, which shows mean transit time versus CBV for three individuals.

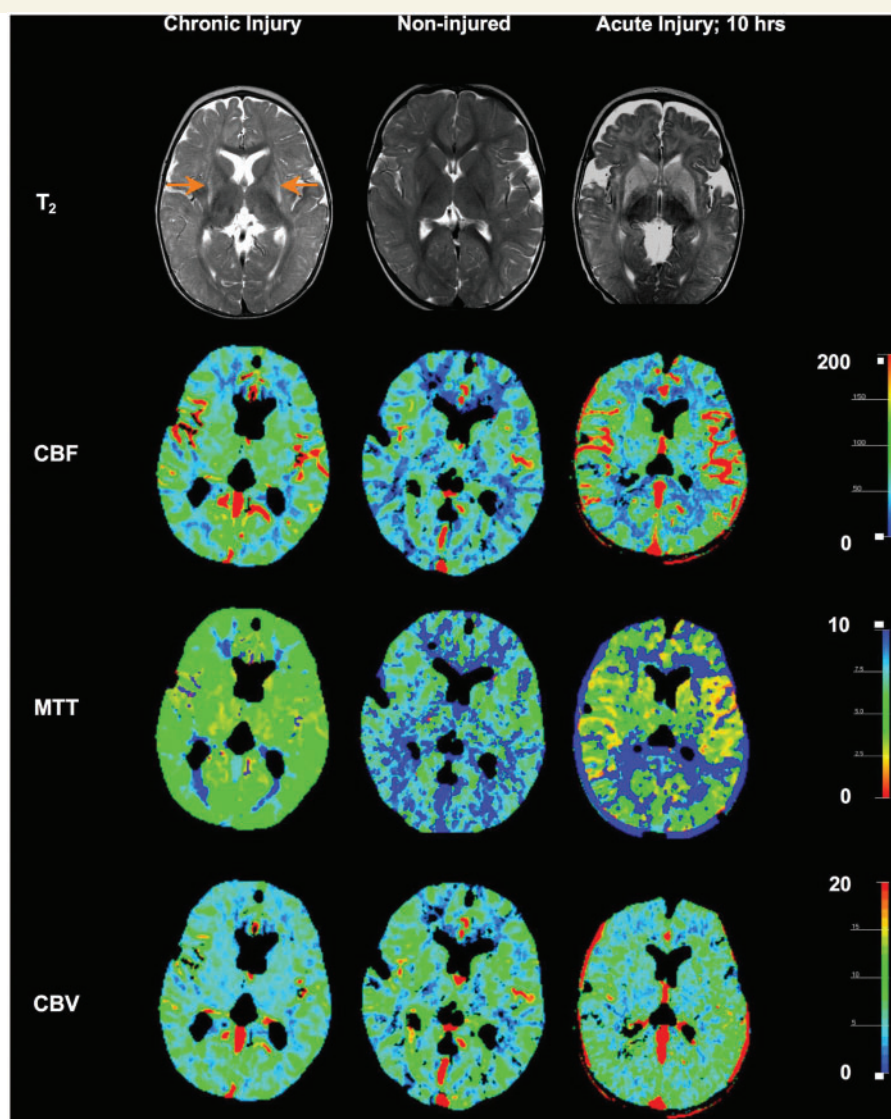


Figure 8 Representative T₂ and corresponding perfusion CT images from GA1 patients in three clinical groups: chronic brain injury (atrophic phase, left column), non-injured (middle column) and acute cytotoxic phase of striatal necrosis (right column). MTT = mean transit time.

Discussion

Cerebral haemodynamics and the glutaric aciduria type 1 toxidrome

In healthy children, cerebral growth, synaptic activity and substrate consumption surge over the first few years of life (Chugani and Phelps, 1991; Johnston, 1995, 2003; Nishino *et al.*, 1997; Erecinska *et al.*, 2004; Wintermark *et al.*, 2004). These changes are accompanied by a 3-fold increase of arterial surface area (Fig. 3), a 50–100% increase of MCA blood velocity (Fig. 4), and a 5-fold increase of CBF (Fig. 7). If GCDH deficiency interferes with brain metabolism (Sauer *et al.*, 2005; Strauss *et al.*, 2007; Zinnanti *et al.*, 2007) and flow-metabolism coupling remains intact, metabolic impairment should be reflected by

lower CBF and velocity. This is in fact the case; asymptomatic patients between 6 months and 5 years of age had MCA mean velocities 18–26% below control values (Fig. 4), similar to the 14–28% decrease of glucose tracer uptake measured by positron emission tomography (Strauss *et al.*, 2007).

In large feeding vessels (Fig. 3), slow velocity was offset by increased vessel calibre according to the equation: Flow = (mean velocity)(cross-sectional area). This relationship suggests that an 18%–26% decrease in velocity through an artery with 34%–42% more cross-sectional area would maintain flow near or above normal levels. In capillaries, however, transit time has the predominant effect on flow (Fig. 6) (Hudetz, 1997a). Thus, three patients who had elevated CBV nevertheless had low tissue blood flow due to slow transit (Table 1). These changes appear to affect all grey matter, not just the striatum (Figs 9 and 10). We cannot explain the discrepancy between estimated

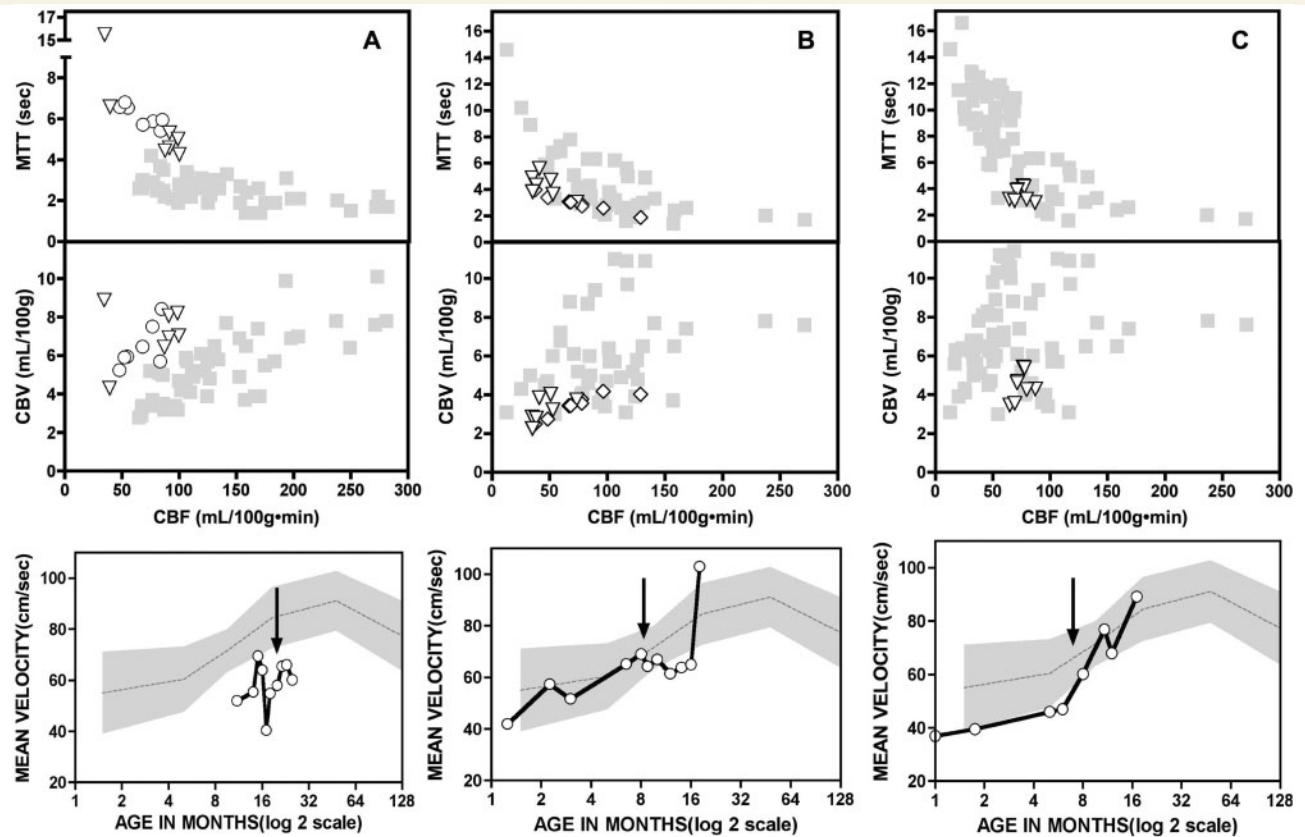


Figure 9 Upper panels show perfusion CT measurements from four children with GA1 (white symbols) compared with nine grey matter regions from age-matched control subjects (grey squares). Perfusion data are plotted as mean transit time (MTT) (seconds) and CBV (mL/100g) against CBF (mL/100 g min). Lower panels depict serial MCA velocity profiles evaluated by serial transcranial colour Doppler ultrasound measurements from these same patients; black arrows indicate timing of perfusion scans. From left to right: (A) two 20-month-old children, one non-injured (white circles) and one injured (white triangles), had prolonged mean transit time (slow velocity), high CBV and low CBF throughout grey matter. The mean transit time/CBF and CBV/CBF ratios were elevated, indicating low perfusion pressure and diminished autoregulatory reserve. (B) Ten hours into acute striatal crisis (white diamonds), an 8-month-old boy had low CBV and short mean transit time (high velocity) with heterogenous striatal CBF values (see Fig. 2). At 100 h (white triangles), CBV remained low and mean transit time had normalized, resulting in more uniform ischaemia throughout deep grey matter. (C) In a 5.5-month-old child with chronic striatal lesions, mean transit time and CBV were low, CBF was normal, and regional perfusion was homogenous.

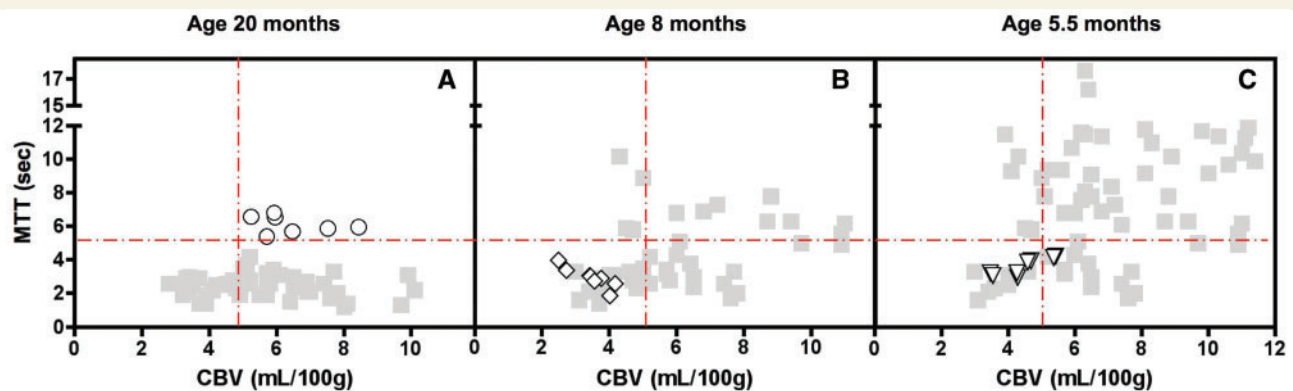


Figure 10 Distinctive perfusion patterns are revealed by plotting grey matter mean transit time (MTT) (seconds) against CBV (mL/100 g), with arbitrary cut points of 5 s and 5 mL/100 g tissue (red dotted lines). Data from age-matched control subjects, plotted as grey squares, show how these variables normally change during development. (A) In a non-injured 20-month-old child, both mean transit time and CBV are high, optimizing substrate exposure and extraction time at any given flow rate. (B) During acute striatal necrosis, a smaller volume of blood moves quickly through the brain. (C) After the striata become atrophic, the CBV and mean transit time remain low relative to CBF.

flow in the MCA (i.e. mean velocity \times cross-sectional area) and measured flow on perfusion scans; these data indicate that an unmeasured fraction of blood may enter the skull and bypass tissue capillaries.

Low CBF and elevated mean transit time are characteristic of many pathological conditions (Ferrari *et al.*, 1992; Bauer *et al.*, 1999; Bristow *et al.*, 2005; Wintermark *et al.*, 2005; Czosnyka *et al.*, 2009), but to our knowledge this is the first report of chronic haemodynamic changes associated with an organic acid disorder. To understand the meaning of these changes better, it is instructive to consider how GCDH deficiency affects brain metabolism. Evidence supports the following model.

- (i) Cerebral production of glutaryl-CoA and derivative organic acids: lysine, in competition with arginine and ornithine, crosses the blood-brain barrier via facilitative cationic amino acid transporters encoded by the genes *SLC7A1* and *SLC7A2* (<http://biogps.gnf.org>) (Smith and Stoll, 1998; Strauss, 2005; Closs *et al.*, 2006; O'Kane *et al.*, 2006; Zinnanti *et al.*, 2007). A small proportion of intracerebral lysine (and tryptophan) constitutively enters the mitochondrial degradation pathway. Glutaryl-CoA, a 5-carbon ester, accumulates proximal to the GCDH block and is a poor substrate for mitochondrial glycine- and acylcarnitine-transferases (Ramsay *et al.*, 2001; Sherman *et al.*, 2008). Based on the biochemical distinction between GA1 and glutaric aciduria type 3, the formation of non-degraded glutaryl-CoA appears essential to biochemical toxicity (Sherman *et al.*, 2008).
- (ii) Toxin entrapment: because glutaryl-CoA and its derivatives (particularly glutarate) do not readily cross the blood-brain barrier (Hassel *et al.*, 2002; Ferreira Gda *et al.*, 2005; Sauer *et al.*, 2006; Keyser *et al.*, 2008), they accumulate to high concentrations within the brain (Funk *et al.*, 2005; Sauer *et al.*, 2006; Zinnanti *et al.*, 2006), where they may inhibit substrate consumption by 15%–30% (Strauss *et al.*, 2007).
- (iii) Threshold energy failure: striatal tissue appears to function adequately in this compromised state provided ATP hydrolysis does not decrease below a minimum threshold (~50%–60% of the normal metabolic rate) necessary to maintain membrane electrical gradients (Erecinska and Silver, 1994; Riepe *et al.*, 1995; Brouillet *et al.*, 1998; Hoshi *et al.*, 2005). However, vulnerable medium spiny neurons can undergo necrotic cell death if this threshold is breached as a result of further metabolic or haemodynamic derangements (Nishino *et al.*, 1997; Brouillet *et al.*, 1998; Calabresi *et al.*, 2000; Nishino *et al.*, 2000).
- (iv) Developmental vulnerability: 'normal' metabolic rate is a dynamic concept; metabolic requirements vary across the brain and change throughout development (Chugani *et al.*, 1991; Chugani and Phelps, 1991; Erecinska *et al.*, 2004). In GA1, striatal necrosis always occurs during the brain's most robust developmental phase, as amino acids are being incorporated into cerebral protein and energy requirements are increasing (Chugani and Phelps, 1991; Strauss, 2005, 2007). During the first few years of life,

higher blood-to-brain lysine transport supports brain protein accretion (Banos, 1978) but also entails potential for more flux through the degradation pathway (Strauss, 2005). Thus, the brain may have its highest content of glutaryl-CoA, glutarate and 3-hydroxyglutarate when it is energetically and haemodynamically most vulnerable (Figs 4 and 6) (Erecinska *et al.*, 2004; Funk *et al.*, 2005; Strauss, 2005).

Because reductions of MCA velocity (Fig. 4) and glucose tracer uptake are comparable (Strauss *et al.*, 2007), we believe that coupling between blood flow and energy metabolism is intact; i.e. that biochemical toxicity entrains the haemodynamic changes. If so, then low velocity (high mean transit time) might compensate for impaired glucose utilization by increasing the time for glucose extraction (Gjedde *et al.*, 1990).

Perfusion pressure and 'metabolic' stroke

We cannot exclude the possibility that haemodynamics play a primary role in 'metabolic' stroke, especially when considering the relationship between flow and velocity. Flow through a blood vessel can be expressed in two different ways, as the product of cross-sectional area and velocity ($Q = \pi r^2 v$) or by the Hagen-Poiseuille equation ($Q = \pi P r^4 / 8 \eta l$) (Despopoulos and Silbernagl, 2003), where Q is flow, r is vessel radius, l is vessel length, η is blood viscosity and P is perfusion pressure, the difference between arterial blood pressure and cerebral venous pressure (Auer and Sutherland, 2002). Combining these equations reveals the relationship between velocity and perfusion pressure: $v = P r^2 / 8 \eta l$.

Assuming relatively constant path length (l) and viscosity (η) under our study conditions, as well as preservation or increase of vessel radius (r ; Fig. 3), low MCA velocity in non-injured children is likely to reflect decreased cerebral perfusion pressure (Fig. 4) (Czosnyka *et al.*, 2009). Two additional observations support this. First, pulsatility tended to be elevated in non-injured patients after 7 months of age (Fig. 5), and studies have shown that MCA pulsatility is inversely related to perfusion pressure (Bellner *et al.*, 2004). Second, CBV and mean transit time were high relative to CBF in some children (Figs 9A and 10A). This pattern (elevated mean transit time/CBF and CBV/CBF ratios) typically indicates arteriolar dilation, increased CBV and low perfusion pressure (Gibbs *et al.*, 1984; Lewis *et al.*, 2001); it raises the important question of autoregulatory reserve in GA1.

As perfusion pressure changes, cerebral autoregulation maintains constant CBF by altering the tone of arterioles (Fig. 12) (Wahl and Schilling, 1993; Lewis *et al.*, 2001; Czosnyka *et al.*, 2009; Schmidt *et al.*, 2009). Maximum arteriolar dilation defines the limit of autoregulation beyond which further reductions of perfusion pressure—due either to reduced systemic blood pressure or increased tissue pressure—reduce CBF (Brady *et al.*, 2009; Czosnyka *et al.*, 2009; Schmidt *et al.*, 2009; Zweifel *et al.*, 2009). Our results suggest that some non-injured patients may live at the brink of this autoregulatory limit (Figs. 4, 5, 7,

9A and 10A), placing them at risk for ischaemic brain injury (Ferrari *et al.*, 1992; Derdeyn *et al.*, 2002).

Haemodynamics, hydrodynamics and haemorrhage

Reduced perfusion pressure can result from systemic hypotension, arteriolar dilation, increased tissue and cerebral venous pressure, or some combination of these (Fig. 12). We did not systematically measure blood pressure in study subjects and although cerebrospinal fluid pressure was high in one neonate (Case 1, Fig. 1), this observation is insufficient to generalize. There are, however, some clues as to the mechanism of reduced perfusion pressure in GA1. Most children with GA1 have a dilated vein of Galen (Strauss *et al.*, 2007) and some suffer intradural and retinal haemorrhages (Martinez-Lage, 1996; Morris *et al.*, 1999). Young lysine-fed *Gcdh*^{−/−} mice develop cerebral venous congestion and haemorrhages in parallel with striatal lesions (Zinnanti *et al.*, 2006). Non-injured patients have high CBV (Table 1, Fig. 9A), about 80% of which is venous (Powers, 1994). Together, these observations suggest that cerebral venous volume and pressure are elevated in both mice and humans with GCDH deficiency (Fig. 12).

In the brain, elevated venous pressure impedes resorption of interstitial fluid (Johanson *et al.*, 2008), which communicates with CSF through gaps in the glia limitans (Fig. 12). This increases both interstitial and CSF fluid volume (Reulen *et al.*, 1977; Rosenberg *et al.*, 1982; Makkat 2003). In GA1 patients of all ages, regardless of injury status, T₂ hyperintensity and high water diffusion in periventricular white matter around the frontal and occipital horns (Fig. 11), medial lemniscus, pallidum and dentate nucleus might indicate interstitial (i.e. vasogenic) oedema (Reulen *et al.*, 1977; Strauss *et al.*, 2003, 2007; Twomey *et al.*, 2003; Harting *et al.*, 2009). These regions may simply function as conduits for bulk transport of interstitial fluid from brain to CSF (Fig. 12) (Pasquini *et al.*, 1977; Rosenberg *et al.*, 1982; Takei *et al.*, 1987; Hunt *et al.*, 2003). This could explain why most GA1 patients who have abnormal subcortical and brainstem white matter signals do not have clinical signs of white matter disease (Strauss *et al.*, 2003; Twomey *et al.*, 2003; Harting *et al.*, 2009).

Increased cerebral venous volume and its relationship to the interstitial fluid compartment (Fig. 12) can tie together several puzzling phenomena in GA1, including increased CSF expansion in neonates (Fig. 1) (Mandel *et al.*, 1991; Martinez-Lage, 1996; Hernandez-Palazon *et al.*, 2006), intradural fluid and blood collections (Martinez-Lage, 1996; Strauss *et al.*, 2003; Twomey *et al.*, 2003), retinal bleeding (Knapp *et al.*, 2002; Gago *et al.*, 2003), dilation of the deep cerebral veins (Zinnanti *et al.*, 2006; Strauss *et al.*, 2007), white matter vacuolization (Soffer *et al.*, 1992; Zinnanti *et al.*, 2006; Harting *et al.*, 2009) and increased brain weight (Strauss, 2005). Along these lines, it is interesting to note that the presenting complaint of an adult-onset GA1 patient—headache (Bahr *et al.*, 2002)—is more suggestive of venous congestion or idiopathic intracranial hypertension than leukodystrophy

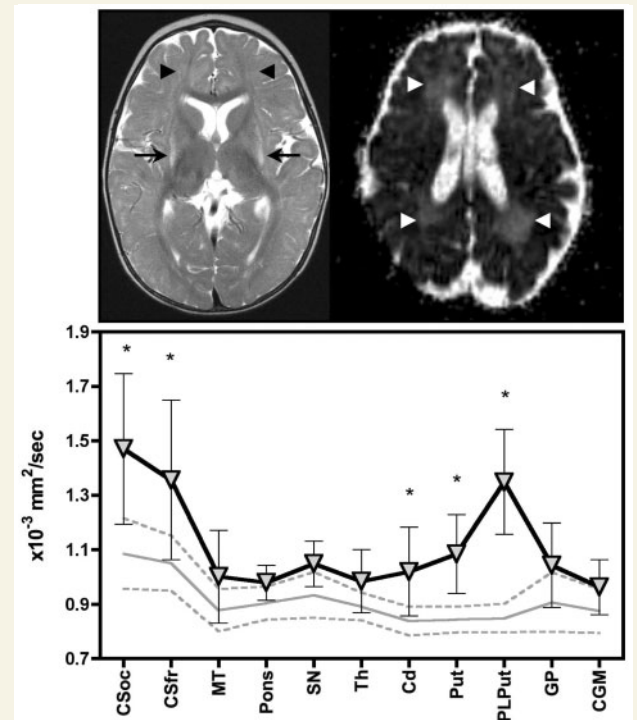


Figure 11 Apparent diffusion coefficients ($\times 10^{-3} \text{ mm}^2/\text{s}$; mean \pm SD) for 11 brain regions (see key below) in 18 GA1 patients with chronic atrophic striatal lesions compared with values of 14 control children ages 7–36 months (control mean \pm SD grey lines; redrawn from original data of Strauss *et al.*, 2007). Individuals with GA1 have elevated water diffusion in the caudate, anterior putamen and posterior-lateral putamen that corresponds to neuronal loss and reactive gliosis (arrows). However, water diffusion tends to be increased throughout the brain, particularly in deep white matter of the centrum semiovale (arrowheads). In older GA1 patients, these deep white matter areas typically show mild symmetrically increased T₂ and fluid attenuated inversion recovery signal intensity. Elevated extrastriatal diffusion values may reflect a generalized expansion of the interstitial space within the brain, most prominent within deep white matter. CSfr = centrum semiovale-frontal; CSoc = centrum semiovale-occipital; MT = large myelin tracks (average of middle cerebellar peduncle = genu and splenium of corpus callosum); Pons = dorsal pontine reticular formation; SN = substantia nigra; Th = thalamus; Cd = caudate; Put = anterior putamen; PLPut = posterior-lateral putamen; GP = globus pallidus; CGM = average of cortical, parietal, and occipital grey matter. Asterisks denote regions where GA1 and control values differ ($P < 0.005$).

(Dahlerup *et al.*, 1985; Tisell *et al.*, 2003; Owler *et al.*, 2005; Mullen *et al.*, 2008; Pujari *et al.*, 2008).

What happens to blood flow during a striatal crisis?

During the acute phase of striatal degeneration, there was a fundamental change in the character of blood flow (Table 1, Figs 2

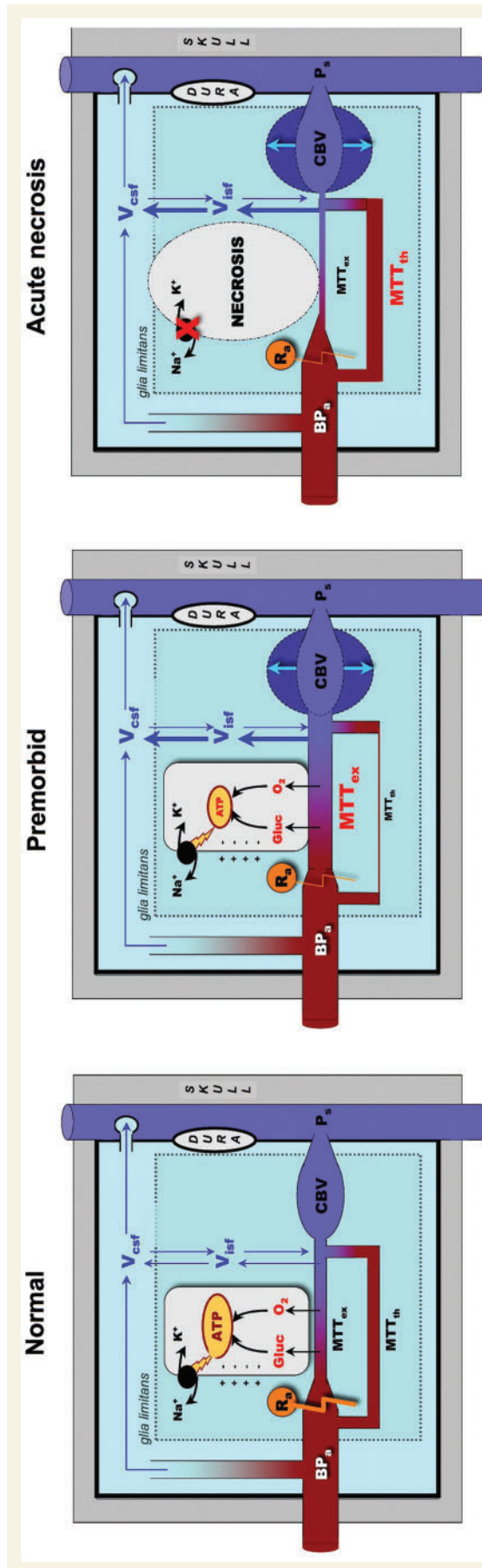


Figure 12 Left panel: under normal conditions, approximately half of the ATP energy generated by mitochondria is used to operate NaK-ATPase and maintain transmembrane electrochemical gradients. The blood flow that delivers glucose and oxygen to tissue is determined by the perfusion pressure—arterial blood pressure (BP_a) minus venous (intracranial) pressure—and the resistance of arterioles (R_a). Two parallel capillary populations, exchange vessels (MTT_{ex}) and non-exchanging thoroughfare channels (MTT_{th}), may carry blood through tissue. In the normal state, exchange vessels—which are under autoregulatory control and have higher mean transit time (MTT)—carry the majority of flow. Although thoroughfare channels probably originate after resistance arterioles, they are drawn pre-arteriolar in the figure to emphasize that they do not exhibit normal autoregulation *in vivo* (see Hudetz 1997a, b). The cerebral veins constitute about 80% of CBV and are influenced by interstitial fluid pressure and dural sinus pressure (P_s). Volume and pressure within the venous system affect the net production of interstitial fluid (V_{isf}). This fluid surrounds nerves and glia and communicates with cerebrospinal fluid (V_{csf}) through gaps in the glia limitans. Middle panel: the premorbid state is characterized by higher blood volume and slower transit. We propose that a primary metabolic disturbance reduces ATP production rate, which entrains arteriolar dilation (reduced R_a) and proportionally higher flow through exchange capillaries. These changes maximize the time for substrate extraction at any given flow rate, but result in higher venous volume and pressure; the latter can increase net production of interstitial fluid and constitutes a risk for intradural and retinal haemorrhages. Right panel: further metabolic (e.g. fever) or haemodynamic (e.g. hypotension) challenges can reduce ATP production below a critical threshold, causing refractory depolarization and cytotoxic swelling. Under these conditions, heterogeneous flow and fast transit may reflect redistribution of blood to thoroughfare channels.

and 9B) which might reflect regional perfusion pressure gradients (Reulen *et al.*, 1977; Vollmar *et al.*, 1999) or capillary redistribution. Hudetz (1997a, b) hypothesized that non-exchanging 'thoroughfare channels' with high velocity and no autoregulation run in parallel with true functional capillaries in the brain (Fig. 12). Thoroughfare channels carry a smaller fraction of total flow so that perfusion characteristics *in vivo* are more indicative of functional (i.e. autoregulating) capillaries.

Because both exchange and thoroughfare channels contribute to measured perfusion, a shift in relationships among CBV, mean transit time and CBF (e.g. Figs 9B and 10B) may signify a shift in the distribution of flow between them. In non-injured children, blood might flow preferentially through exchange capillaries to optimize 'functional' capillary density and glucose extraction time (Gjedde *et al.*, 1990). If metabolic activity of striatal neurons declines suddenly, flow may redistribute to non-exchanging vessels (Fig. 9B) (Hudetz, 1997a). Transcranial Doppler data support this idea. Brain-injured children had relative increases of MCA velocity between 6 and 18 months and reduced velocity thereafter (Fig. 4). This surge appears after the brain is injured (Fig. 9B and C) and may depict transient uncoupling of flow and metabolism in damaged tissue. A similar phenomenon occurs immediately after an occlusive stroke; upon reperfusion, nutrient and oxygen flow to necrotic tissue greatly exceed metabolic demand (Gjedde *et al.*, 1990).

Clinical implications of haemodynamic changes in glutaric aciduria type 1

We are now in a position to imagine a chain of events that culminates in striatal degeneration: (i) glutaryl-CoA and its derivatives, glutarate and 3-hydroxyglutarate, are constitutively produced by, and accumulate within, GCDH-deficient brain cells (Strauss, 2005; Sauer *et al.*, 2006; Zinnanti *et al.*, 2007); (ii) entrapped metabolites interfere with cerebral energy metabolism, detected as a 25%–30% reduction of striatal fluorodeoxyglucose uptake (Strauss *et al.*, 2007); (iii) metabolic toxicity entrains haemodynamic changes that decrease capillary blood velocity (increase substrate transit time), increase CBV and maintain flow-metabolism coupling; (iv) MCA perfusion pressure is reduced, most likely as a result of arteriolar dilation, resulting in venous congestion and elevated interstitial fluid pressure (Fig. 12); and (v) physiologic conditions which increase energy requirements (e.g. fever) (Laptook and Corbett, 2002), decrease energy supply (e.g. hypoglycaemia), threaten perfusion (e.g. dehydration, hypotension, intracranial hypertension), or produce these problems in combination, could decrease striatal energy turnover below a critical threshold and lead to necrosis. Such a model suggests that 'metabolic stroke' arises from a complex interplay of metabolic and haemodynamic phenomena, as has been proposed for other histotoxins such as 3-nitropropionic acid, cyanide and carbon monoxide (Chyi and Chang, 1999; Auer and Sutherland, 2002).

Our model assumes that metabolic toxicity is the primary cause of developmental brain injury and secondary haemodynamic changes amplify the risk. This means that intravenous infusions

during illnesses, prescribed to provide 10–12 mg/kg min of dextrose and about 150% the maintenance fluid requirement, might have two important therapeutic actions: to increase dextrose delivery to the brain and to increase cerebral perfusion pressure. These data also explain age-related susceptibility; the risk for brain injury subsides following the brain's natural plateau of energy expenditure, protein accretion and blood flow (Figs 4 and 7).

This study opens up new areas for clinical investigation. Measurement of MCA velocity and cerebral perfusion in a culturally and genetically broader group will reveal if cerebrovascular patterns are related to genotype or biochemical phenotype. Such validation is essential before our findings can be generalized to the larger GA1 population. Longitudinal studies could more closely analyse the relationship between MCA velocity and neurological risk, similar to the strategy used for sickle cell anaemia (Adams, 2007). However, our preliminary findings suggest that Doppler data may be an imperfect tool for this purpose because of marked intra-individual variation over time (Fig. 9, lower panels) and considerable overlap between injured and non-injured patients.

Future haemodynamic studies should include measurement of arterial blood pressure and might also examine velocity in deep cerebral veins (Valdúeza *et al.*, 1996; Doepp *et al.*, 2006). Given the haemodynamic similarities of GA1 to idiopathic intracranial hypertension (Owler *et al.*, 2005) and high-altitude encephalopathy (Wilson *et al.*, 2009), a more systematic study of retinal pathology in GA1 may be warranted and, when indicated, lumbar puncture should always prompt measurement of opening pressure.

Perfusion CT is a powerful method for interrogating haemodynamics, but it is logistically difficult in children and involves small, but measurable, radiation exposure (Wintermark *et al.*, 2001, 2004). Advances in magnetic resonance imaging (Olivot *et al.*, 2009; Zaharchuk *et al.*, 2009) should increase the number of perfusion studies that can be done safely in children. More extensive perfusion imaging in a variety of clinical settings will be necessary to determine how specific treatment variables (e.g. lysine-restricted diet, L-carnitine etc.) affect brain physiology. If blood flow changes are indeed linked to the biochemical status of striatal neurons, interventions that decrease cerebral production of glutaryl-CoA should improve cerebral energetics and produce measurable increases in MCA velocity and brain perfusion.

Acknowledgements

The authors thank Dr Holmes Morton for his clinical and scientific insights, and Drs Julie Mack and James Eastman III, for constructive suggestions during the preparation of the manuscript. Dr Alan Shuldiner graciously donated ultrasound services used for this study. The staff of Lancaster General Hospital and the MRI Group were indispensable for obtaining high quality images. Finally, we thank our patients, our most important teachers, to whom this work is dedicated.

Funding

This study was funded in part by charitable donations from the Amish and Mennonite communities to the Clinic for Special Children.

Supplementary material

Supplementary material is available at *Brain* online.

References

- Abe K, Yoshimura H, Tanaka H, Fujita N, Hikita T, Sakoda S. Comparison of conventional and diffusion-weighted MRI and proton MR spectroscopy in patients with mitochondrial encephalomyopathy, lactic acidosis, and stroke-like events. *Neuroradiology* 2004; 46: 113–7.
- Adams RJ. Big strokes in small persons. *Arch Neurol* 2007; 64: 1567–74.
- Auer RN, Sutherland GR. Hypoxia and related conditions. In: Graham DI, Lantos PL, editors. *Greenfield's neuropathology*. Vol. 1. London: Arnold; 2002. p. 233–80.
- Bahr O, Mader I, Zschocke J, Dichgans J, Schulz JB. Adult onset glutaric aciduria type I presenting with a leukoencephalopathy. *Neurology* 2002; 59: 1802–4.
- Bauer R, Bergmann R, Walter B, Brust P, Zwiener U, Johannsen B. Regional distribution of cerebral blood volume and cerebral blood flow in newborn piglets – effect of hypoxia/hypercapnia. *Brain Res Dev Brain Res* 1999; 112: 89–98.
- Bellner J, Romner B, Reinstrup P, Kristiansson KA, Ryding E, Brandt L. Transcranial Doppler sonography pulsatility index (PI) reflects intracranial pressure (ICP). *Surg Neurol* 2004; 62: 45–51, discussion 51.
- Bennett MJ, Marlow N, Pollitt RJ, Wales JK. Glutaric aciduria type 1: biochemical investigations and postmortem findings. *Eur J Pediatr* 1986; 145: 403–5.
- Brady KM, Lee JK, Kibler KK, Easley RB, Koehler RC, Czosnyka M, et al. The lower limit of cerebral blood flow autoregulation is increased with elevated intracranial pressure. *Anesth Analg* 2009; 108: 1278–83.
- Bristow MS, Simon JE, Brown RA, Eliasziw M, Hill MD, Coutts SB, et al. MR perfusion and diffusion in acute ischemic stroke: human gray and white matter have different thresholds for infarction. *J Cereb Blood Flow Metab* 2005; 25: 1280–7.
- Brouillet E, Guyot MC, Mittoux V, Altairac S, Conde F, Palfi S, et al. Partial inhibition of brain succinate dehydrogenase by 3-nitropropionic acid is sufficient to initiate striatal degeneration in rat. *J Neurochem* 1998; 70: 794–805.
- Calabresi P, Centonze D, Bernardi G. Cellular factors controlling neuronal vulnerability in the brain: a lesson from the striatum. *Neurology* 2000; 55: 1249–55.
- Chugani HT, Hovda DA, Villablanca JR, Phelps ME, Xu WF. Metabolic maturation of the brain: a study of local cerebral glucose utilization in the developing cat. *J Cereb Blood Flow Metab* 1991; 11: 35–47.
- Chugani HT, Phelps ME. Imaging human brain development with positron emission tomography. *J Nucl Med* 1991; 32: 23–6.
- Chyi T, Chang C. Temporal evolution of 3-nitropropionic acid-induced neurodegeneration in the rat brain by T2-weighted, diffusion-weighted, and perfusion magnetic resonance imaging. *Neuroscience* 1999; 92: 1035–41.
- Closs EI, Boissel JP, Habermeier A, Rotmann A. Structure and function of cationic amino acid transporters (CATs). *J Membr Biol* 2006; 213: 67–77.
- Czosnyka M, Brady K, Reinhard M, Smielewski P, Steiner LA. Monitoring of cerebrovascular autoregulation: facts, myths, and missing links. *Neurocrit Care* 2009; 10: 373–86.
- Dahlerup B, Gjerris F, Harmsen A, Sorensen PS. Severe headache as the only symptom of long-standing shunt dysfunction in hydrocephalic children with normal or slit ventricles revealed by computed tomography. *Childs Nerv Syst* 1985; 1: 49–52.
- Derdeyn CP, Videen TO, Yundt KD, Fritsch SM, Carpenter DA, Grubb RL, et al. Variability of cerebral blood volume and oxygen extraction: stages of cerebral haemodynamic impairment revisited. *Brain* 2002; 125: 595–607.
- Despopoulos A, Silbernagl S. *Color atlas of physiology*. New York: Thieme; 2003.
- Doepp F, Valdueza JM, Schreiber SJ. Serial ultrasound assessment of the basal vein of Rosenthal in HSV encephalitis. *Ultrasound Med Biol* 2006; 32: 473–7.
- Erecinska M, Cherian S, Silver IA. Energy metabolism in mammalian brain during development. *Prog Neurobiol* 2004; 73: 397–445.
- Erecinska M, Silver IA. Ions and energy in mammalian brain. *Prog Neurobiol* 1994; 43: 37–71.
- Feeke JA, Cassell MD. The vascular supply of the functional compartments of the human striatum. *Brain* 2006; 129: 2189–201.
- Ferrari M, Wilson DA, Hanley DF, Traystman RJ. Effects of graded hypotension on cerebral blood flow, blood volume, and mean transit time in dogs. *Am J Physiol* 1992; 262: H1908–14.
- Ferreira Gda C, Viegas CM, Schuck PF, Tonin A, Ribeiro CA, Coelho Dde M, et al. Glutaric acid administration impairs energy metabolism in midbrain and skeletal muscle of young rats. *Neurochem Res* 2005; 30: 1123–31.
- Funk CB, Prasad AN, Frosk P, Sauer S, Kolker S, Greenberg CR, et al. Neuropathological, biochemical and molecular findings in a glutaric acidemia type 1 cohort. *Brain* 2005; 128: 711–22.
- Gago LC, Wegner RK, Capone A Jr., Williams GA. Intraretinal hemorrhages and chronic subdural effusions: glutaric aciduria type 1 can be mistaken for shaken baby syndrome. *Retina* 2003; 23: 724–6.
- Gibbs JM, Wise RJ, Leenders KL, Jones T. Evaluation of cerebral perfusion reserve in patients with carotid-artery occlusion. *Lancet* 1984; 1: 310–4.
- Gjedde A, Kuwabara H, Hakim AM. Reduction of functional capillary density in human brain after stroke. *J Cereb Blood Flow Metab* 1990; 10: 317–26.
- Goodman SI, Norenberg MD, Shikes RH, Breslich DJ, Moe PG. Glutaric aciduria: biochemical and morphologic considerations. *J Pediatr* 1977; 90: 746–50.
- Haas RH, Marsden DL, Capistrano-Estrada S, Hamilton R, Grafe MR, Wong W, et al. Acute basal ganglia infarction in propionic acidemia. *J Child Neurol* 1995; 10: 18–22.
- Harting I, Neumaier-Probst E, Seitz A, Maier EM, Assmann B, Baric I, et al. Dynamic changes of striatal and extrastriatal abnormalities in glutaric aciduria type I. *Brain* 2009; 132: 1764–82.
- Hassel B, Brathe A, Petersen D. Cerebral dicarboxylate transport and metabolism studied with isotopically labelled fumarate, malate and malonate. *J Neurochem* 2002; 82: 410–9.
- Hernandez-Palazon J, Sanchez-Rodenas L, Martinez-Lage JF, Collado IC. Anesthetic management in two siblings with glutaric aciduria type 1. *Paediatr Anaesth* 2006; 16: 188–91.
- Hoffmann GF, Gibson KM, Trefz FK, Nyhan WL, Bremer HJ, Rating D. Neurological manifestations of organic acid disorders. *Eur J Pediatr* 1994; 153: S94–100.
- Hoshi A, Nakahara T, Ogata M, Yamamoto T. The critical threshold of 3-nitropropionic acid-induced ischemic tolerance in the rat. *Brain Res* 2005; 1050: 33–9.
- Hudetz AG. Blood flow in the cerebral capillary network: a review emphasizing observations with intravital microscopy. *Microcirculation* 1997a; 4: 233–52.
- Hudetz AG. Regulation of oxygen supply in the cerebral circulation. *Adv Exp Med Biol* 1997b; 428: 513–20.
- Hunt RW, Warfield SK, Wang H, Kean M, Volpe JJ, Inder TE. Assessment of the impact of the removal of cerebrospinal fluid on cerebral tissue volumes by advanced volumetric 3D-MRI in posthaemorrhagic hydrocephalus in a premature infant. *J Neurol Neurosurg Psychiatry* 2003; 74: 658–60.

- Johanson CE, Duncan JA 3rd, Klinge PM, Brinker T, Stopa EG, Silverberg GD. Multiplicity of cerebrospinal fluid functions: New challenges in health and disease. *Cerebrospinal Fluid Res* 2008; 5: 10.
- Johnston MV. Neurotransmitters and vulnerability of the developing brain. *Brain Dev* 1995; 17: 301–6.
- Johnston MV. Injury and plasticity in the developing brain. *Exp Neurol* 2003; 184 Suppl 1: S37–41.
- Keyser B, Glatzel M, Stellmer F, Kortmann B, Lukacs Z, Kolker S, et al. Transport and distribution of 3-hydroxyglutaric acid before and during induced encephalopathic crises in a mouse model of glutaric aciduria type 1. *Biochim Biophys Acta* 2008; 1782: 385–90.
- Knapp JF, Soden SE, Dasouki MJ, Walsh IR. A 9-month-old baby with subdural hematomas, retinal hemorrhages, and developmental delay. *Pediatr Emerg Care* 2002; 18: 44–7.
- Kolker S, Hoffmann GF, Schor DS, Feyh P, Wagner L, Jeffrey I, et al. Glutaryl-CoA dehydrogenase deficiency: region-specific analysis of organic acids and acylcarnitines in post mortem brain predicts vulnerability of the putamen. *Neuropediatrics* 2003; 34: 253–60.
- Kolker S, Koeller DM, Sauer S, Horster F, Schwab MA, Hoffmann GF, et al. Excitotoxicity and bioenergetics in glutaryl-CoA dehydrogenase deficiency. *J Inher Metab Dis* 2004; 27: 805–12.
- Laptook AR, Corbett RJ. The effects of temperature on hypoxic-ischemic brain injury. *Clin Perinatol* 2002; 29: 623–49, vi.
- Lewis SB, Wong ML, Bannan PE, Piper IR, Reilly PL. Transcranial Doppler identification of changing autoregulatory thresholds after autoregulatory impairment. *Neurosurgery* 2001; 48: 369–75; discussion 375–6.
- Mandel H, Braun J, el-Peleg O, Christensen E, Berant M. Glutaric aciduria type I. Brain CT features and a diagnostic pitfall. *Neuroradiology* 1991; 33: 75–8.
- Martinez-Lage JF. Neurosurgical treatment for hydrocephalus, subdural hematomas, and arachnoid cysts in glutaric aciduria type 1. *Neuropediatrics* 1996; 27: 335–6.
- Morris AA, Hoffmann GF, Naughten ER, Monavari AA, Collins JE, Leonard JV. Glutaric aciduria and suspected child abuse. *Arch Dis Child* 1999; 80: 404–5.
- Morton DH, Bennett MJ, Seargeant LE, Nichter CA, Kelley RI. Glutaric aciduria type I: a common cause of episodic encephalopathy and spastic paralysis in the Amish of Lancaster County, Pennsylvania. *Am J Med Genet* 1991; 41: 89–95.
- Muhlhausen C, Ergun S, Strauss KA, Koeller DM, Crnic L, Woontner M, et al. Vascular dysfunction as an additional pathomechanism in glutaric aciduria type I. *J Inher Metab Dis* 2004; 27: 829–34.
- Mullen MT, Sansing LH, Hurst RW, Weigle JB, Polasani RS, Messe SR. Obstructive Hydrocephalus from Venous Sinus Thrombosis. *Neurocrit Care* 2008.
- Nishino H, Hida H, Kumazaki M, Shimano Y, Nakajima K, Shimizu H, et al. The striatum is the most vulnerable region in the brain to mitochondrial energy compromise: a hypothesis to explain its specific vulnerability. *J Neurotrauma* 2000; 17: 251–60.
- Nishino H, Kumazaki M, Fukuda A, Fujimoto I, Shimano Y, Hida H, et al. Acute 3-nitropropionic acid intoxication induces striatal astrocytic cell death and dysfunction of the blood-brain barrier: involvement of dopamine toxicity. *Neurosci Res* 1997; 27: 343–55.
- O’Kane RL, Vina JR, Simpson I, Zaragoza R, Mokashi A, Hawkins RA. Cationic amino acid transport across the blood-brain barrier is mediated exclusively by system y⁺. *Am J Physiol Endocrinol Metab* 2006; 291: E412–9.
- Olivot JM, Mlynash M, Zaharchuk G, Straka M, Bammer R, Schwartz N, et al. Perfusion MRI (Tmax and MTT) correlation with xenon CT cerebral blood flow in stroke patients. *Neurology* 2009; 72: 1140–5.
- Oppenheim C, Galanaud D, Samson Y, Sahel M, Dormont D, Wechsler B, et al. Can diffusion weighted magnetic resonance imaging help differentiate stroke from stroke-like events in MELAS? *J Neurol Neurosurg Psychiatry* 2000; 69: 248–50.
- Owler BK, Parker G, Halmagyi GM, Johnston IH, Besser M, Pickard JD, et al. Cranial venous outflow obstruction and pseudotumor Cerebri syndrome. *Adv Tech Stand Neurosurg* 2005; 30: 107–74.
- Pasquini U, Bronzini M, Gozzoli E, Mancini P, Menichelli F, Salvolini U. Periventricular hypodensity in hydrocephalus: a clinico-radiological and mathematical analysis using computed tomography. *J Comput Assist Tomogr* 1977; 1: 443–8.
- Powers WJ. Positron Emission Tomography of the Brain. In: Bevan RD, Bevan JA, editors. *The Human Brain Circulation: Functional Changes in Disease*. Totowa, N.J.: Humana Press; 1994. p. 1–22.
- Pujari S, Kharkar S, Metellus P, Shuck J, Williams MA, Rigamonti D. Normal pressure hydrocephalus: long-term outcome after shunt surgery. *J Neurol Neurosurg Psychiatry* 2008; 79: 1282–6.
- Ramsay RR, Gandour RD, van der Leij FR. Molecular enzymology of carnitine transfer and transport. *Biochim Biophys Acta* 2001; 1546: 21–43.
- Reulen HJ, Graham R, Spatz M, Klatzo I. Role of pressure gradients and bulk flow in dynamics of vasogenic brain edema. *J Neurosurg* 1977; 46: 24–35.
- Riepe MW, Hori N, Ludolph AC, Carpenter DO. Failure of neuronal ion exchange, not potentiated excitation, causes excitotoxicity after inhibition of oxidative phosphorylation. *Neuroscience* 1995; 64: 91–7.
- Rosenberg GA, Kyner WT, Estrada E. The effect of increased CSF pressure on interstitial fluid flow during ventriculocisternal perfusion in the cat. *Brain Res* 1982; 232: 141–50.
- Sauer SW, Okun JG, Fricker G, Mahringer A, Muller I, Crnic LR, et al. Intracerebral accumulation of glutaric and 3-hydroxyglutaric acids secondary to limited flux across the blood-brain barrier constitute a biochemical risk factor for neurodegeneration in glutaryl-CoA dehydrogenase deficiency. *J Neurochem* 2006; 97: 899–910.
- Sauer SW, Okun JG, Schwab MA, Crnic LR, Hoffmann GF, Goodman SI, et al. Bioenergetics in glutaryl-coenzyme A dehydrogenase deficiency: a role for glutaryl-coenzyme A. *J Biol Chem* 2005; 280: 21830–6.
- Schmidt B, Klingelhofer J, Perkes I, Czosnyka M. Cerebral autoregulatory response depends on the direction of change in perfusion pressure. *J Neurotrauma* 2009; 26: 651–6.
- Sherman EA, Strauss KA, Tortorelli S, Bennett MJ, Knerr I, Morton DH, et al. Genetic mapping of glutaric aciduria, type 3, to chromosome 7 and identification of mutations in c7orf10. *Am J Hum Genet* 2008; 83: 604–9.
- Smith QR, Stoll JS. Blood-brain barrier amino acid transport. In: Pardridge WM, editor. *Introduction to the Blood-Brain Barrier*. Vol. 1. Cambridge: Cambridge University Press; 1998. p. 188–97.
- Soffer D, Amir N, Elpeleg ON, Gomori JM, Shalev RS, Gottschalk-Sabag S. Striatal degeneration and spongy myelinopathy in glutaric acidemia. *J Neurol Sci* 1992; 107: 199–204.
- Strauss KA. Glutaric aciduria type 1: a clinician’s view of progress. *Brain* 2005; 128: 697–9.
- Strauss KA, Lazovic J, Wintermark M, Morton DH. Multimodal imaging of striatal degeneration in Amish patients with glutaryl-CoA dehydrogenase deficiency. *Brain* 2007; 130: 1905–20.
- Strauss KA, Morton DH. Type I glutaric aciduria, part 2: a model of acute striatal necrosis. *Am J Med Genet C Semin Med Genet* 2003; 121: 53–70.
- Strauss KA, Puffenberger EG, Robinson DL, Morton DH. Type I glutaric aciduria, part 1: natural history of 77 patients. *Am J Med Genet C Semin Med Genet* 2003; 121: 38–52.
- Takei F, Shapiro K, Kohn I. Influence of the rate of ventricular enlargement on the white matter water content in progressive feline hydrocephalus. *J Neurosurg* 1987; 66: 577–83.
- Tisell M, Tullberg M, Hellstrom P, Blomsterwall E, Wikkelso C. Neurological symptoms and signs in adult aqueductal stenosis. *Acta Neurol Scand* 2003; 107: 311–7.
- Twomey EL, Naughten ER, Donoghue VB, Ryan S. Neuroimaging findings in glutaric aciduria type 1. *Pediatr Radiol* 2003; 33: 823–30.
- Valdúez JM, Schmierer K, Mehraein S, Einhaupl KM. Assessment of normal flow velocity in basal cerebral veins. A transcranial doppler ultrasound study. *Stroke* 1996; 27: 1221–5.

- Vollmar B, Westermann S, Menger MD. Microvascular response to compartment syndrome-like external pressure elevation: an in vivo fluorescence microscopic study in the hamster striated muscle. *J Trauma* 1999; 46: 91–6.
- Wahl M, Schilling L. Regulation of cerebral blood flow – a brief review. *Acta Neurochir Suppl (Wien)* 1993; 59: 3–10.
- Wilson MH, Newman S, Imray CH. The cerebral effects of ascent to high altitudes. *Lancet Neurol* 2009; 8: 175–91.
- Wintermark M, Cotting J, Roulet E, Lepori D, Meuli R, Maeder P, et al. Acute brain perfusion disorders in children assessed by quantitative perfusion computed tomography in the emergency setting. *Pediatr Emerg Care* 2005; 21: 149–60.
- Wintermark M, Lepori D, Cotting J, Roulet E, van Melle G, Meuli R, et al. Brain perfusion in children: evolution with age assessed by quantitative perfusion computed tomography. *Pediatrics* 2004; 113: 1642–52.
- Wintermark M, Thiran JP, Maeder P, Schnyder P, Meuli R. Simultaneous measurement of regional cerebral blood flow by perfusion CT and stable xenon CT: a validation study. *AJNR Am J Neuroradiol* 2001; 22: 905–14.
- Zaharchuk G, Bammer R, Straka M, Shankaranarayan A, Alsop DC, Fischbein NJ, et al. Arterial spin-label imaging in patients with normal bolus perfusion-weighted MR imaging findings: pilot identification of the borderzone sign. *Radiology* 2009; 252: 797–807.
- Zinnanti WJ, Lazovic J, Housman C, LaNoue K, O'Callaghan JP, Simpson I, et al. Mechanism of age-dependent susceptibility and novel treatment strategy in glutaric acidemia type I. *J Clin Invest* 2007; 117: 3258–70.
- Zinnanti WJ, Lazovic J, Wolpert EB, Antonetti DA, Smith MB, Connor JR, et al. A diet-induced mouse model for glutaric aciduria type I. *Brain* 2006; 129: 899–910.
- Zweifel C, Czosnyka M, Lavinio A, Castellani G, Kim DJ, Carrera E, et al. A comparison study of cerebral autoregulation assessed with transcranial Doppler and cortical laser Doppler flowmetry. *Neurol Res* 2009. Advance Access published on August 21, 2009.